

2

INJURY BIOMECHANICS RESEARCH *Proceedings of the Eighth International Workshop*

PROBLEMS OF MEASUREMENT IN HUMAN ANALOG RESEARCH

Leonard Lustick, Gerald Williamson, Marjorie Seemann and James Bartholomew

INTRODUCTION

The Naval Biodynamics Laboratory in New Orleans is involved in a continuing effort to describe the kinematic and physiological response of anatomical segments of human volunteers to acceleration environments (1,2,3).^{*} The scope of this presentation is to discuss some of the problems that arise in the measurement of the three dimensional dynamic response of human volunteers to relatively short duration (250 millisecond) acceleration profiles.

At the outset of the program it was recognized that redundant measurement systems would be required to measure all levels of the dynamic response (acceleration to displacement) with the desired accuracy and to check the results of each measurement system. Initial studies had indicated that accelerometer derived kinematic variables would be the best source of angular and linear acceleration components, whereas the angular orientation and linear displacement components which are obtained directly from photo data (rather than by integration) would be most accurate for these latter variables. Further, if special care is used in the selection and calibration of the accelerometers (4) angular and linear velocity components derived from accelerometer data will compare favorably with those derived from photo data in the time window of interest (250 milliseconds).

* Numbers in parentheses indicate References at end of paper.

PROBLEMS OF MEASUREMENT IN HUMAN ANALOG RESEARCH

In keeping with this, the dynamic response of anatomical segments at the Naval Biodynamics Laboratory is measured with accelerometer configurations, cinephotography and gyros. The accelerometers and cinephotography techniques are complete systems allowing the three dimensional motion of a rigid body to be described. The gyro configuraton only measures two components of angular velocity and is used for monitoring the experimental runs and for validation where applicable (5,6).

It was always the intention to finally combine the measurements from the redundant measurement systems in an "optimum" fashion and consequently represent the dynamic response at all levels (acceleration to displacement) in one consistent "best" set of data. Subsequently, preliminary results of a method to accomplish this optimum combination are presented. A more complete description of the method and its utilization will be presented in a future paper.

PHOTO PROBLEMS

The target configurations at the Naval Biodynamics Laboratory are attached to a rigid body and are tracked by at least two cameras. The displacement and orientation of the rigid body are determined with a least squares algorithm using the target locations in the film plane as well as the measured location and orientation of the cameras in the laboratory. At the NBDL, the coordinates of the targets in the film plane are

PROBLEMS OF MEASUREMENT IN HUMAN ANALOG RESEARCH

determined by an automatic digitizing system. The system in general is good, but editing is required to remove macroscopic errors such as misidentification of targets and crossing targets. It has been found useful to plot the target configuration determined by the film coordinates as seen from each camera (25 frames per page) to locate and to correct if possible these macroscopic errors. As an illustration Figure 1 shows 25 frames of a particular run. In addition to editing, this method allows a quick look at the motion as seen by the camera.

To process photo data it is required to have a transformation from points in the object plane to points in the film plane. This requires accurate calibration of each camera and accurate determination of the location and camera orientation in the laboratory. At the NBDL an optical bench with a plane of photo targets and an Azimuth/Elevation pedestal for the camera is dedicated to the determination of individual camera calibration parameters. It is important to realize that there may be significant differences between cameras.

Low frequency errors due to camera orientation, position or calibration constants result in sharp discontinuities in the least square photo solutions when the target configuration changes due to drop-out or additions of targets. These discontinuities

PROBLEMS OF MEASUREMENT IN HUMAN ANALOG RESEARCH

are accentuated in areas where the solution is sensitive to errors. In order to hold these discontinuities to a minimum, the errors in determination of camera calibration constants, and camera location and orientation should be minimized. In addition, a computation procedure for smoothing the discontinuities may be required. An algorithm that is based on a weighted average of past and current target residuals has been developed at the NBDL to remove these discontinuities.

COMPARISON OF PHOTO AND ACCELEROMETER DERIVED ANGULAR VELOCITY

The accelerometer derived variables at the NBDL are derived from a six accelerometer configuration with sensitive axes orientation and accelerometer location as shown in Figure 2 (6). The six accelerometer system has been much maligned in favor of redundant nine accelerometer configurations. Figures 3 through 6 present angular velocity around the anatomical Y axis for an increasing sequence of peak G levels (5G to 10G) for -Gx runs derived from a six accelerometer configuration arranged as shown in Figure 2.

The problem is three dimensional, but only the significant component of angular velocity for these -Gx runs is shown. Figures 7 through 18 are a continuation of this sequence for 13G and 14G peak sled acceleration. A three triad accelerometer configuration was used for these runs. The three triads were formed by adding accelerometers where required to make each triad similar to the triad shown in Figure 2. Three dimensional components of angular velocity were determined both from a least square algorithm for the three triad nine accelerometers and the six accelerometer configuration shown in Figure 2.

PROBLEMS OF MEASUREMENT IN HUMAN ANALOG RESEARCH

Figures 7 and 8 compare the angular velocity component around the anatomical Y axis derived from the three triad (nine accelerometers) and six accelerometers respectively for the 13G run. This is the significant component of angular velocity for the -Gx runs and as seen from these figures very little difference exists between the six and nine accelerometer solutions and both agree well with the photo derived angular velocity. A similar comparison is shown for the angular velocity components around the anatomical X axis in Figures 9 and 10 and the anatomical Z axis in Figures 11 and 12. These same comparisons are shown for a 14G run in Figures 13 through 18. The solution for the nine accelerometers is better than that for the six accelerometers for the small angular velocity components around the anatomical X and Z axes. This is as expected since there is a statistical advantage with the nine accelerometers and the error in either case is significant relative to the magnitude of the angular velocity for these components in a -Gx run. It should be noticed that the profiles for the six and the nine accelerometer solutions are very similar and there is no evidence of unstable "blow up" in either case.

SIMULATION STUDIES

A program has been developed at the NBDL to evaluate the effect of low frequency accelerometer errors (sensitivity, orientation and linearity) on the errors in kinematic variables derived from these measurements. This program uses the solution of the kinematic variables to generate realistic errors in each of the accelerometers. The solutions obtained with the accelerometers modified by the errors are compared with those obtained from the unmodified accelerometer measurements. In this way, the sensitivity to errors of accelerometer derived kinematic variables is evaluated consistent with

PROBLEMS OF MEASUREMENT IN HUMAN ANALOG RESEARCH

the type of acceleration profile being studied at the NBDL. Investigation of this sort for (-X), (+Y) and (-X, +Y) vector direction profiles studied at the NBDL have indicated that for errors in accelerometers consistent with pre-selection of accelerometers and the careful calibration procedure there is no blow-up of solutions with six accelerometers. The errors in kinematic variables in the time window of interest (250 milliseconds) are consistent with the error growth due to integrating the errors in angular acceleration resulting from deriving angular acceleration components from linear acceleration measurements. These conclusions are reinforced by the good agreement between photo and accelerometer derived angular velocity components in the actual data base. The simulation studies show that with significantly larger accelerometer errors unstable behavior with six accelerometers is observed. Under these conditions the error grows out of bounds in very short times. This behavior has never been observed in any of the human runs at the NBDL. Simulation studies comparing three triad solutions with six accelerometer solutions have indicated that when the errors in the accelerometers are large enough to cause unstable behavior of the solutions in the time window of interest with six accelerometers, the solutions with the three triad configuration, although stable, is of poor quality.

COMBINATIONS OF PHOTO AND ACCELEROMETER DATA

As mentioned previously, it has always been the intention to combine photo and accelerometer solutions into one "optimum" solution that would provide a consistent set of variables from the acceleration to displacement levels suitable for modeling and mannikin construction.

PROBLEMS OF MEASUREMENT IN HUMAN ANALOG RESEARCH

The solution from photo data although good for displacement and angular orientation, requires extensive signal conditioning in order to derive angular and linear acceleration variables. In addition, there are often gaps in the photo solutions due to inadequate target coverage. In view of this, an algorithm has been devised to use the photo displacement and orientation results to predict errors in the sensitivity and orientation of each accelerometer. This solution uses both the photo derived results and the apriori accelerometer error components. The solution is then obtained using accelerometer data modified as predicted with the above algorithms. A more complete description of this algorithm will be presented in a future paper.

Figures 19 through 24 compare the linear and angular orientation components derived from photo measurements, a six accelerometer configuration and the optimum combination of photo and accelerometers. These results are presented for a $-7G_x$ accelerometer profile. The (+), (X) and (A) plot symbols are consistent with the photo, accelerometer and combined solution, respectively. As can be easily observed, the combined solution is indeed very close to the solution derived from the photo data. Angular velocity comparisons are made in Figures 25 through 27 for this same $-G_x$ run. Changes in linear and angular acceleration components are obtained but are small and are not shown. The method appears encouraging and the authors intend to more fully explore its uses and implementation in the future.

CONCLUSIONS

1. With pre-selection of accelerometers and careful calibration procedures six accelerometer configurations can provide results which agree well with photo-derived results at the velocity level in the time window of interest (250 milliseconds) for the acceleration profiles investigated at the NBDL. The error growth in the time window of interest is consistent with deriving angular acceleration from linear acceleration measurements and integrating the low frequency errors in the accelerometers.
2. Given the same accuracy in accelerometers, there is a statistical advantage of a three triad (nine accelerometer) configuration over a 3-2-1 six accelerometer configuration and the nine accelerometer solution is marginally stable. However, if the errors in the accelerometers are such that the six accelerometer solution exhibits unstable behavior in the time window of interest for acceleration profiles run at the NBDL, then the three triad solution is of poor quality.
3. An algorithm has been developed which combines photo and accelerometer data into one consistent data base. This algorithm uses a model for accelerometer errors and can use non-contiguous photo derived variables to predict the parameters in these models. The kinematic variables are then derived from the accelerometer measurements and the modified parameters associated with each accelerometer.

REFERENCES

- (1) Ewing, C.L., Thomas, D.J., Lustick, L.S., Becker, E.B., Willems, G. and Muzzy, W.H. III, "The Effect of the Initial Position of the Head and Neck on the Dynamic Response of the Human Head and Neck to -Gx Impact Acceleration", Proceedings of the Nineteenth Stapp Car Crash Conference, Society of Automotive Engineers, Inc., Warrendale, PA, 1975.
- (2) Ewing, C.L., Thomas, D.J., Lustick, L.S., Muzzy, W.H.III, Willems, G. and Majewski, P.L., "The Effect on Duration, Rate of Onset and Peak Sled Acceleration on the Dynamic Response of the Human Head and Neck", Proceedings of the Twentieth Stapp Car Crash Conference, Society of Automotive Engineers, Inc., Warrendale, PA, 1976.
- (3) Ewing, C.L., Thomas, D.J., Lustick, L.S., Muzzy, W.H.III, Willems, G. and Majewski, P.L., "Dynamic Response of Human Head and Neck to +Gy Impact Acceleration", Proceedings of the Twenty-First Stapp Car Crash Conference, Society of Automotive Engineers, Inc., Warrendale, PA, 1977.
- (4) Willems, G., 1977 "A Detailed Performance Evaluation of Subminiature Piezoresistive Accelerometers", Twenty-Third International Instrumentation Symposium, Instrument Society of America.
- (5) Becker, E.B., 1975 "A Photographic Data System for Determination of 3-Dimensional Effects of Multi-axes Impact Acceleration on Living Humans", Proceedings, Society of Photo-Optical Instrumentation Engineers, V.57.
- (6) Becker, E.B. and Willems, G., "An Experimentally Validated 3-D Inertial Tracking Package for Application in Biodynamic Research", Proceedings of the Nineteenth Stapp Car Crash Conference, Society of Automotive Engineers, Inc., Warrendale, PA, 1975.

- Figure 1 T-Plate Plots for Editing Photo Data
- Figure 2 Accelerometer Configurations
- Figure 3 Angular Velocity Around Anatomical Y Axis
(-5Gx, 6 Accelerometers)
- Figure 4 Angular Velocity Around Anatomical Y Axis
(-7Gx, 6 Accelerometers)
- Figure 5 Angular Velocity Around Anatomical Y Axis
(-9Gx, 6 Accelerometers)
- Figure 6 Angular Velocity Around Anatomical Y Axis
(-10Gx, 6 Accelerometers)
- Figure 7 Angular Velocity Around Anatomical Y Axis
(-13Gx, 9 Accelerometers)
- Figure 8 Angular Velocity Around Anatomical Y Axis
(-13Gx, 6 Accelerometers)
- Figure 9 Angular Velocity Around Anatomical X Axis
(-13Gx, 9 Accelerometers)
- Figure 10 Angular Velocity Around Anatomical X Axis
(-13Gx, 6 Accelerometers)
- Figure 11 Angular Velocity Around Anatomical Z Axis
(-13Gx, 9 Accelerometers)
- Figure 12 Angular Velocity Around Anatomical Z Axis
(-13Gx, 6 Accelerometers)
- Figure 13 Angular Velocity Around Anatomical Y Axis
(-14Gx, 9 Accelerometers)
- Figure 14 Angular Velocity Around Anatomical Y Axis
(-14Gx, 6 Accelerometers)
- Figure 15 Angular Velocity Around Anatomical X Axis
(-14Gx, 9 Accelerometers)
- Figure 16 Angular Velocity Around Anatomical X Axis
(-14Gx, 6 Accelerometers)
- Figure 17 Angular Velocity Around Anatomical Z Axis
(-14Gx, 9 Accelerometers)

- Figure 18 Angular Velocity Around Anatomical Z Axis
(-14Gx, 6 Accelerometers)
- Figure 19 Comparison of Displacement of Head Anatomical Origin
Relative to the Sled (Laboratory X Direction)
- Figure 20 Comparison of Displacement of Head Anatomical Origin
Relative to the Sled (Laboratory Y Direction)
- Figure 21 Comparison of Displacement of Head Anatomical Origin
Relative to the Sled (Laboratory Z Direction)
- Figure 22 Comparison of Euler Angle Around Head Anatomical X Axis
- Figure 23 Comparison of Euler Angle Around Carried Head Anatomical Y Axis
- Figure 24 Comparison of Euler Angle Around Carried Head Anatomical Z Axis
- Figure 25 Comparison of Angular Velocity Around Head Anatomical X Axis
- Figure 26 Comparison of Angular Velocity Around Head Anatomical Y Axis
- Figure 27 Comparison of Angular Velocity Around Head Anatomical Z Axis

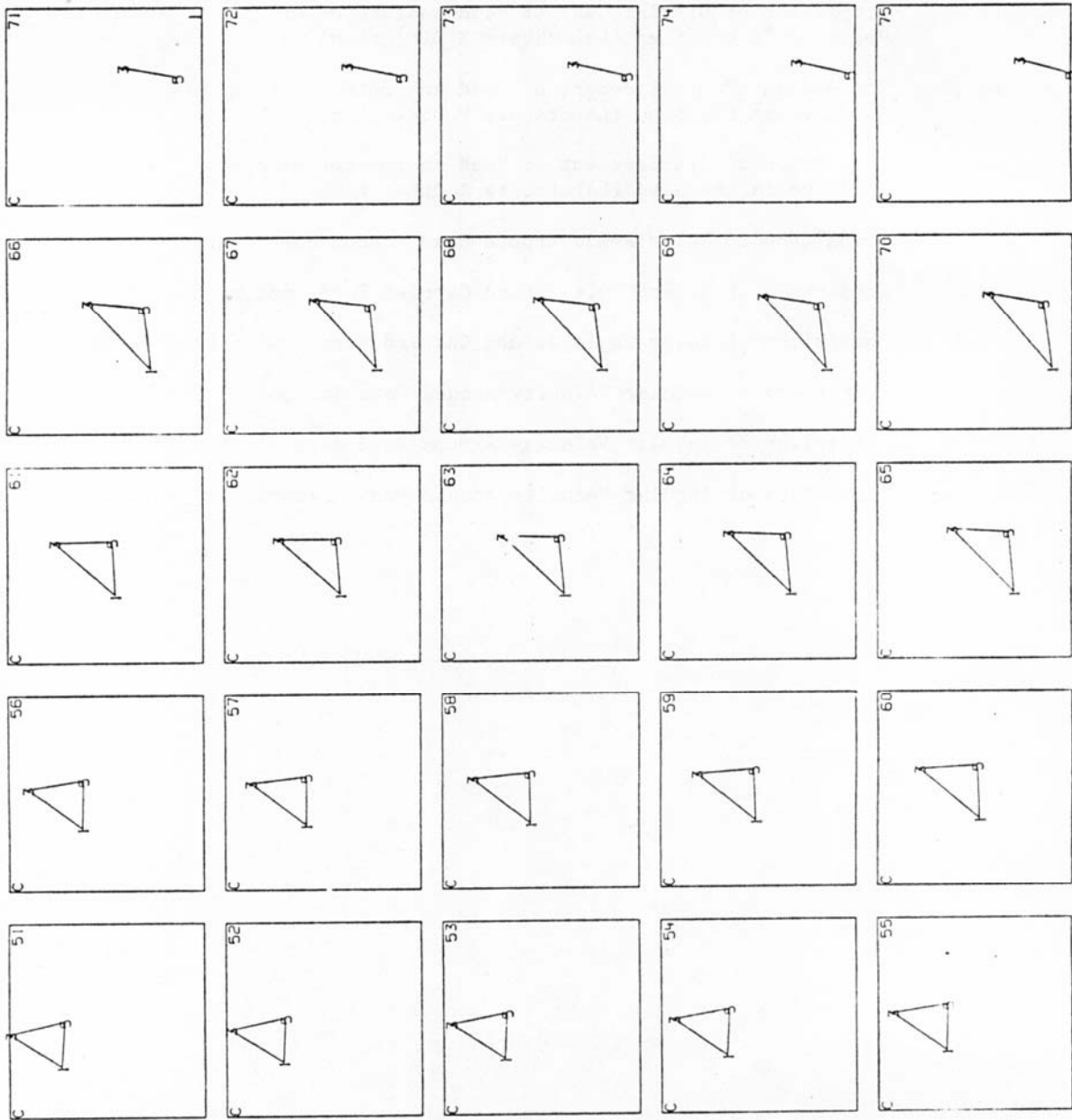


Fig. 1

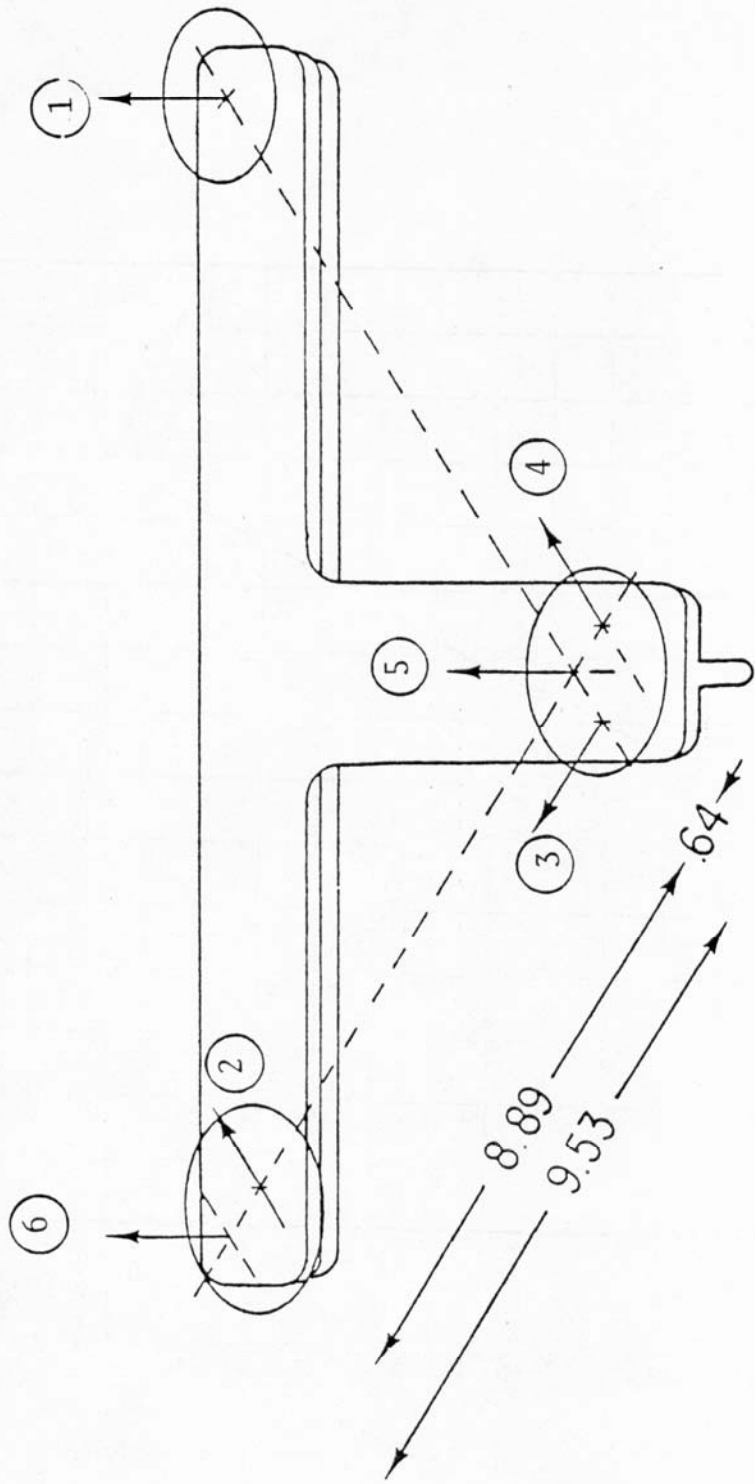


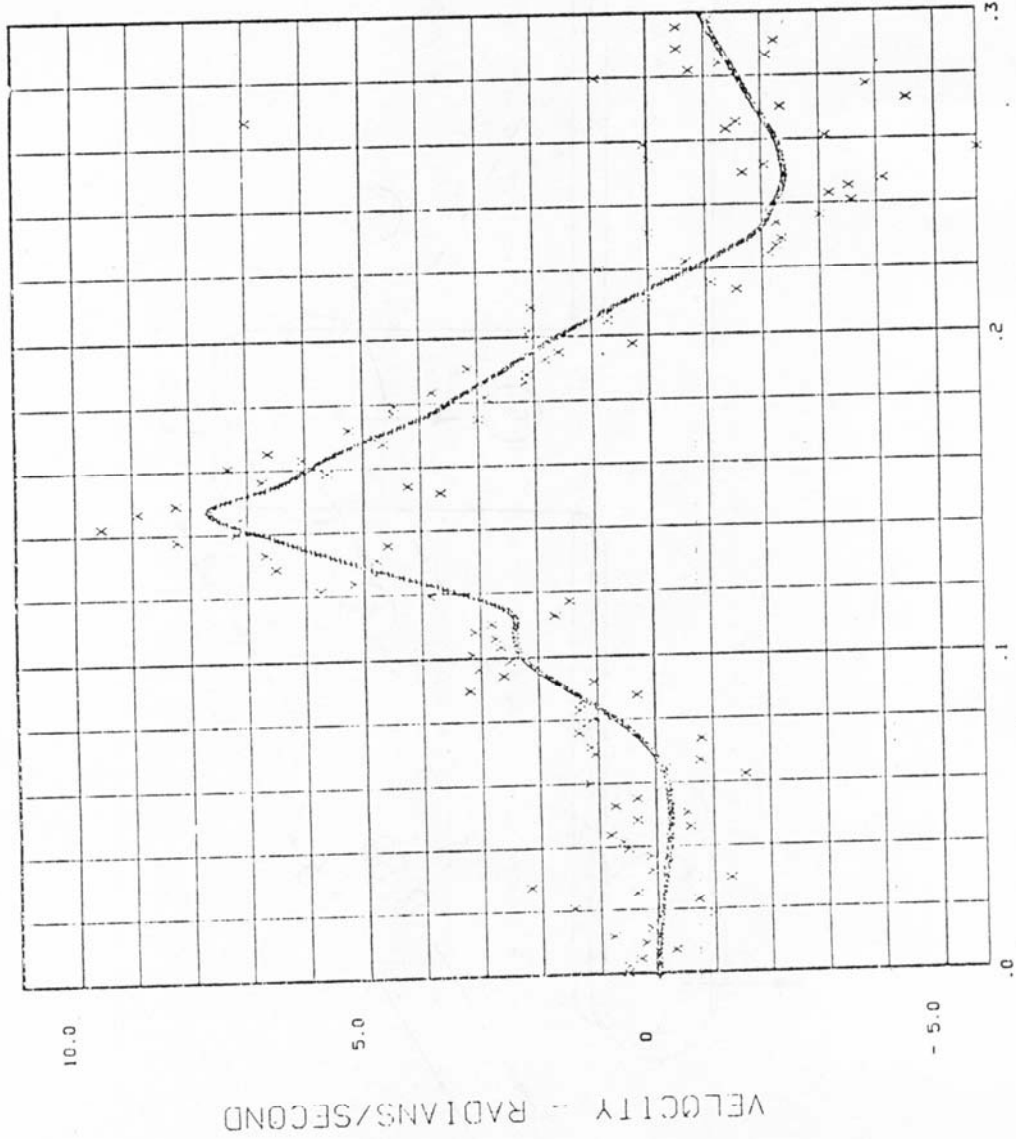
Fig. 2

unfiltered (o)

1029.

.10C4 (X) = RHBOXP.

LXC529 H00108 (+) = RHEOXS



14 MAY 80

TIME - SECONDS

Fig. 3

unfiltered (c)

1561.

71.1

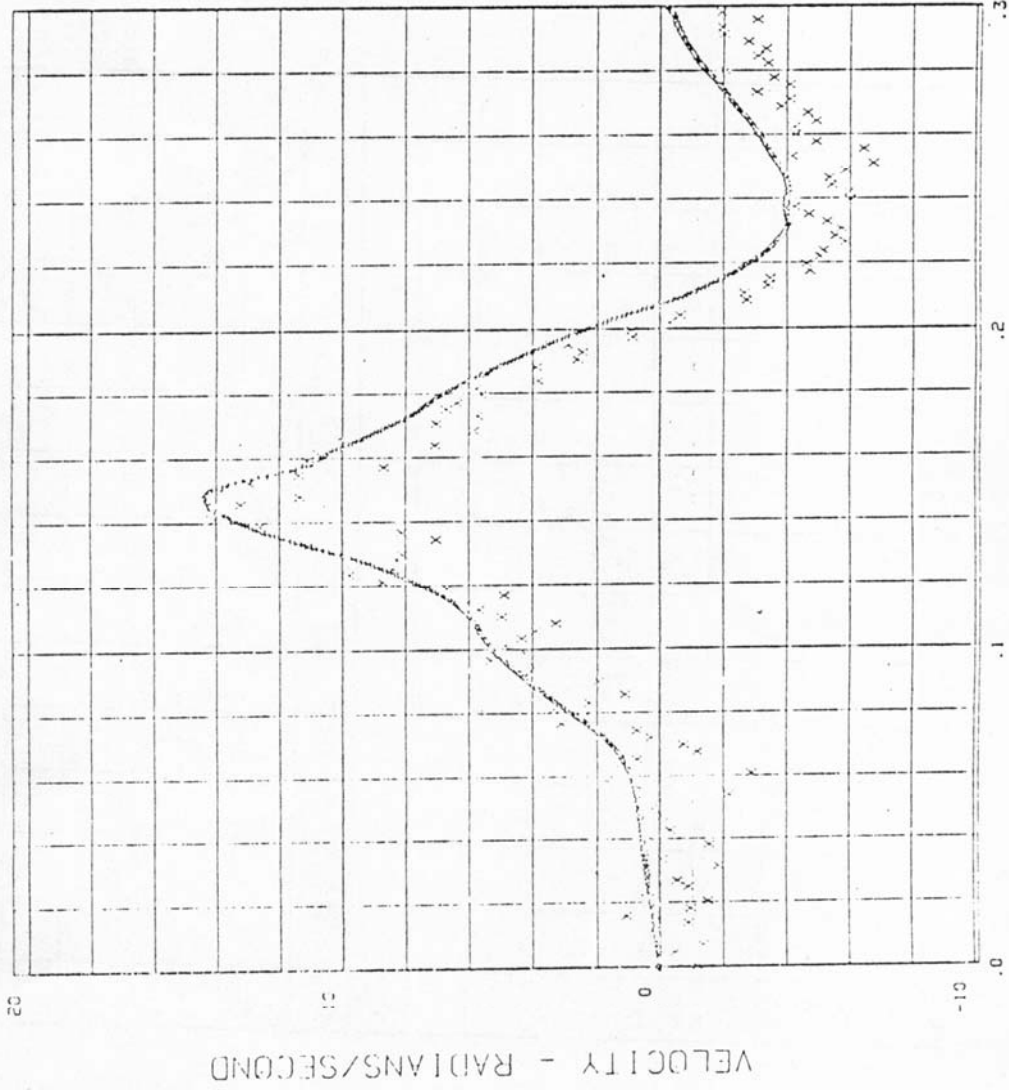
.1013

(X) = RH33XP

H00109

(-) = RH33XS

LXC536



14 MAY 80

TIME - SECONDS

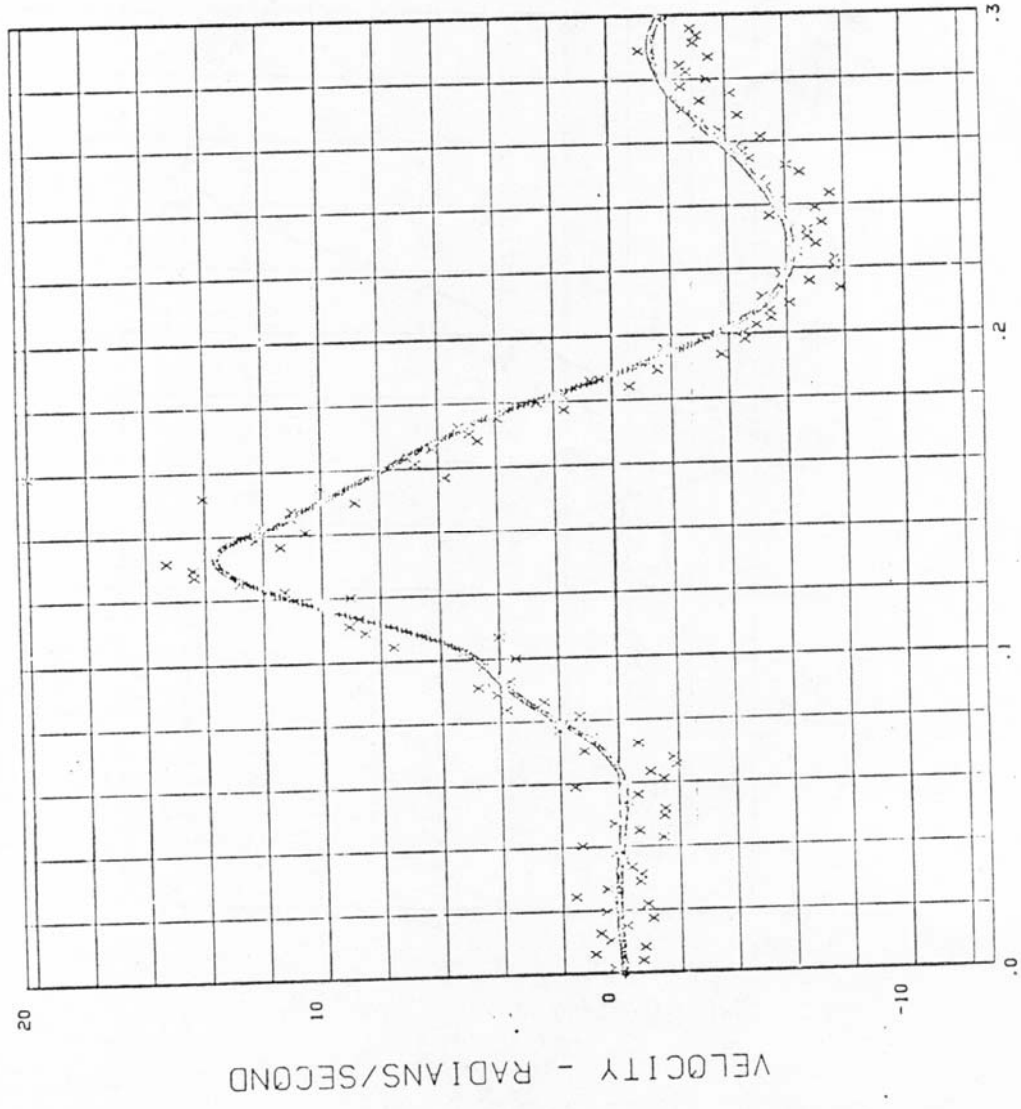
Fig. 4

unfiltered (6)

2126.

.1012 88.5
(X) = RHBOXP

LX3545 H00108
(+) = RHBOXS



28 MAY 80

TIME - SECONDS

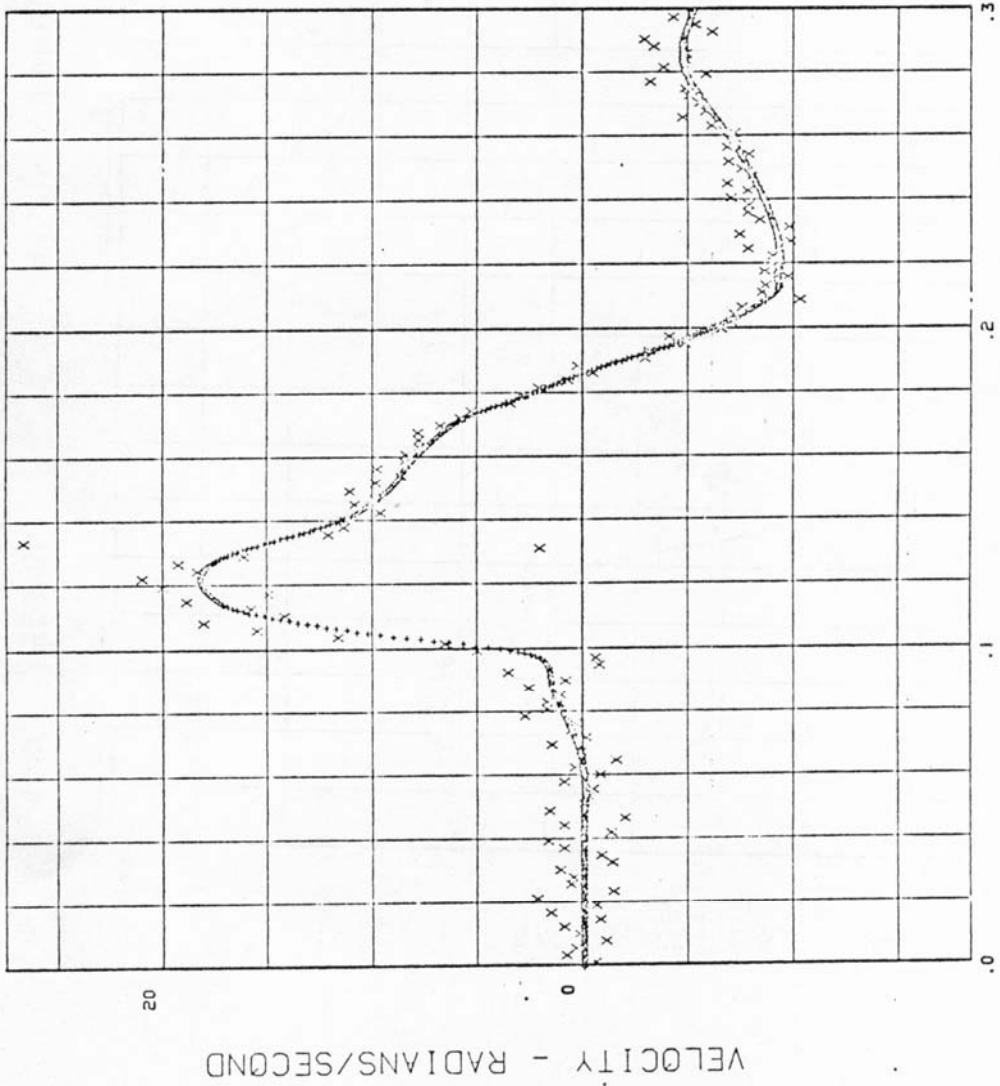
Fig. 5

unfiltered (6)

2550.

.1020 (X) = RHBCXP

LX3551 H00108 (+) = RHBCXS



27 MAY 80

TIME - SECONDS

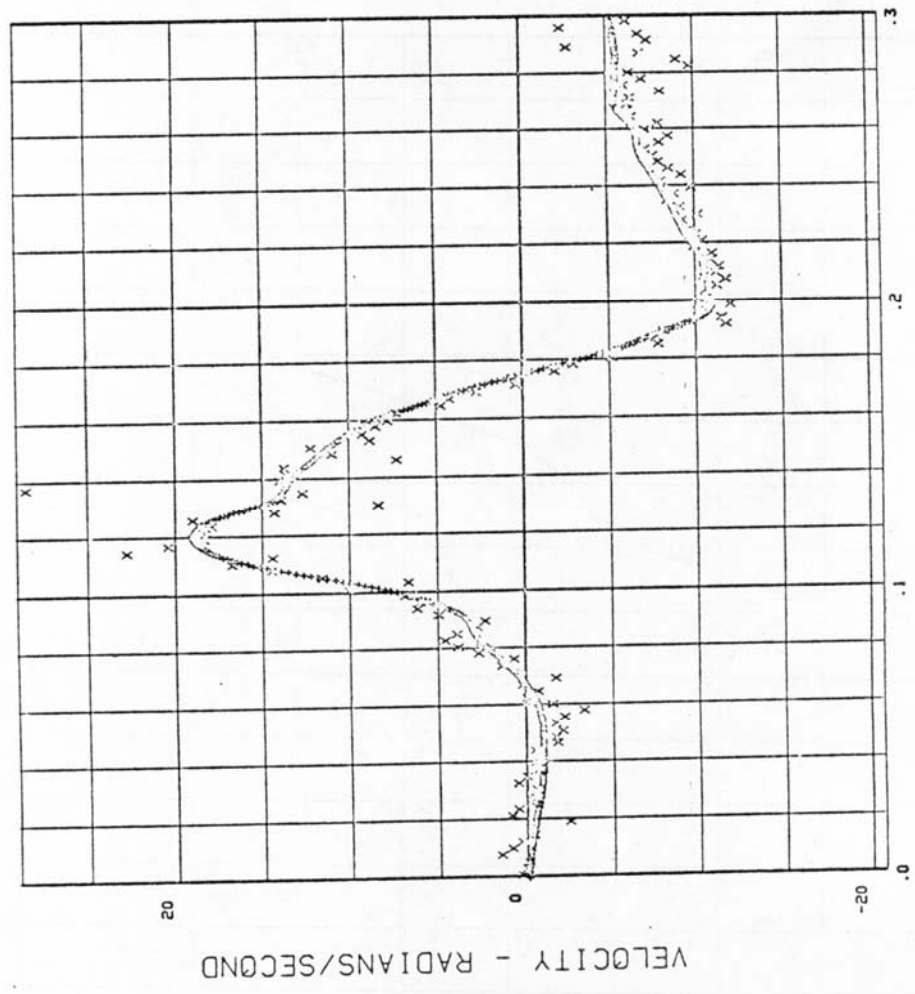
Fig. 6

unfiltered (9)

3860.

.0940 (X) = RHBOXP

LX3579 H00108 (+) = RHBOXS



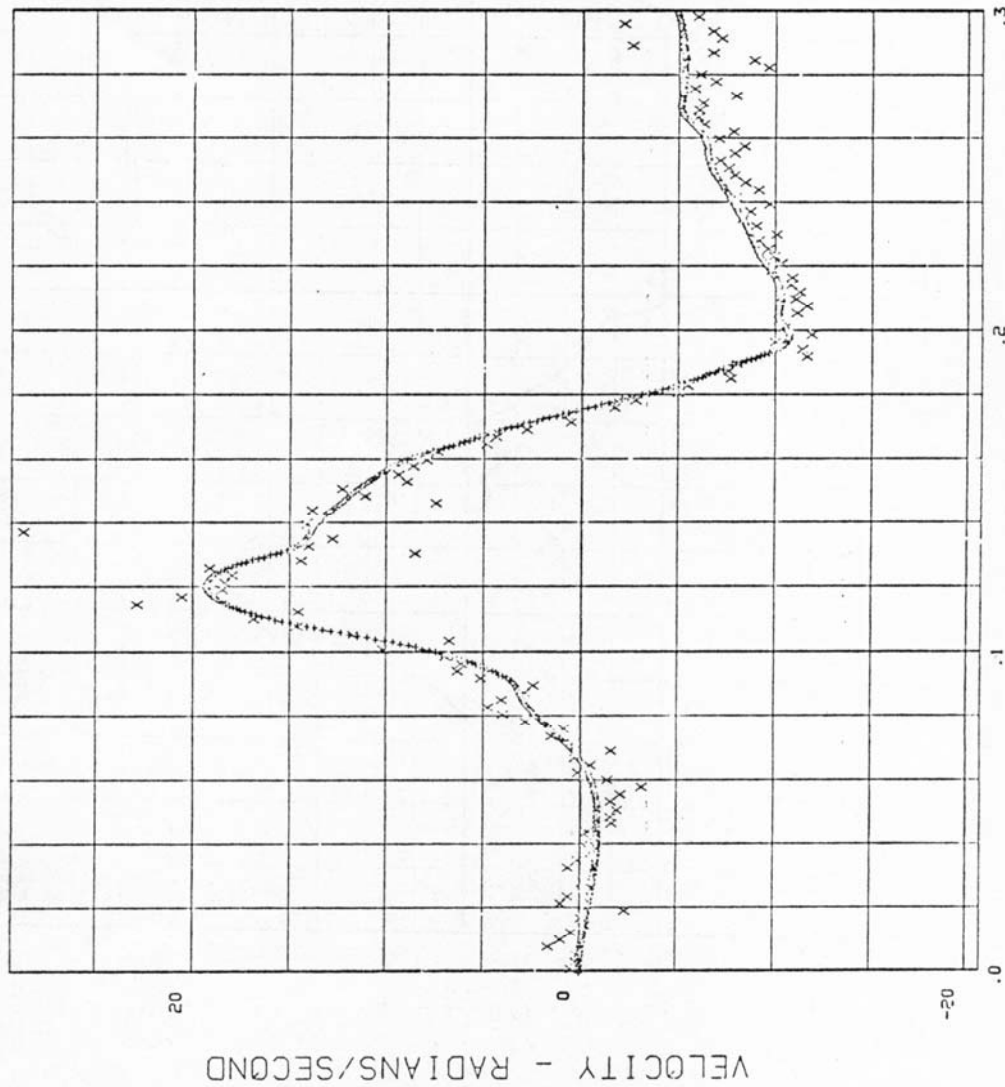
12 JUN 80

TIME - SECONDS

Fig. 7

unfiltered (6)

LX3579 H00108 .0940 129.9 3860.
(+) = RHBOXS (X) = RHBOXP



TIME - SECONDS 18 JUN 80

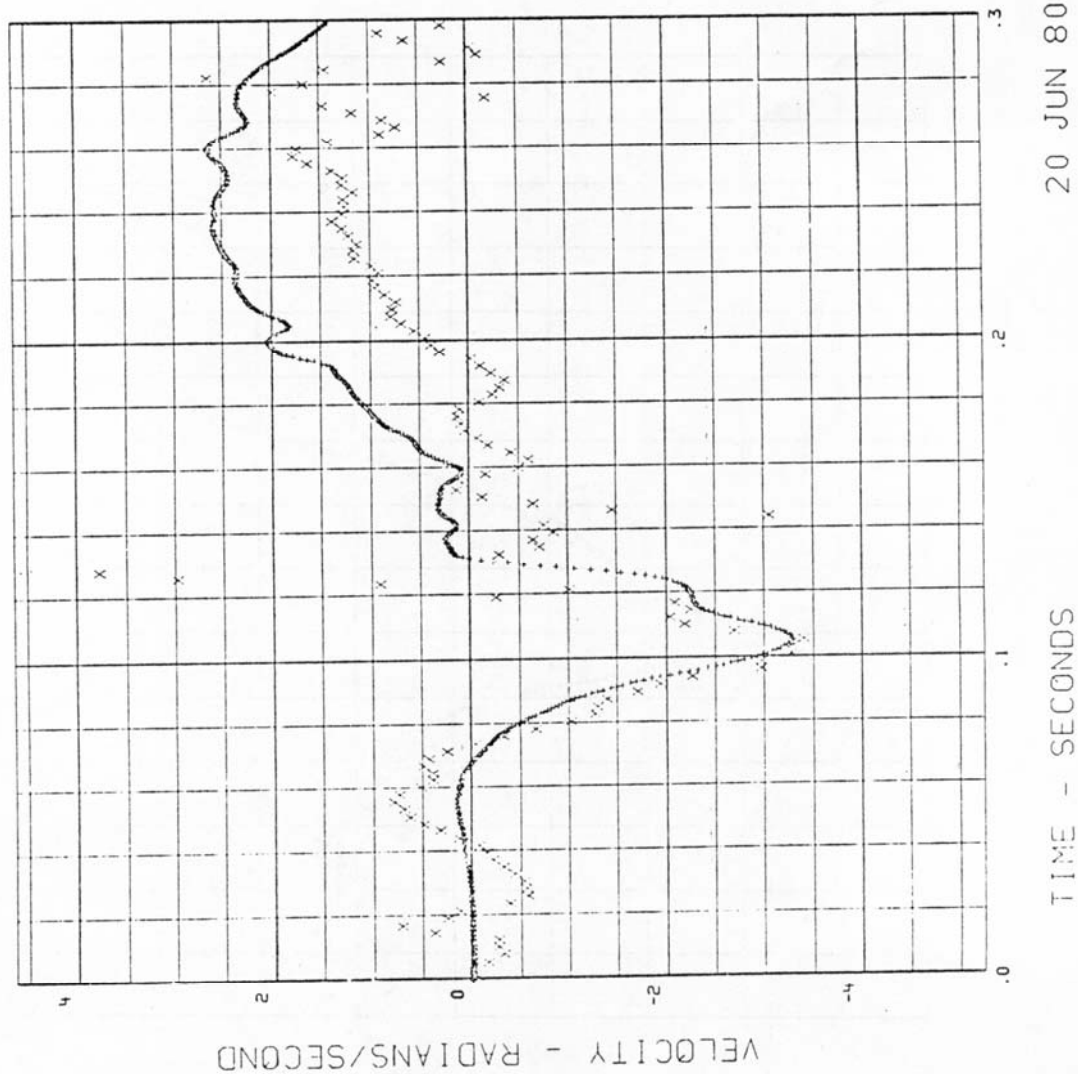
Fig. 8

Filtered (9)

3860.

.0940 129.9
(X) = RHAQXP

LX3579 H00108
(+) = RHAQXS



20 JUN 80

TIME - SECONDS

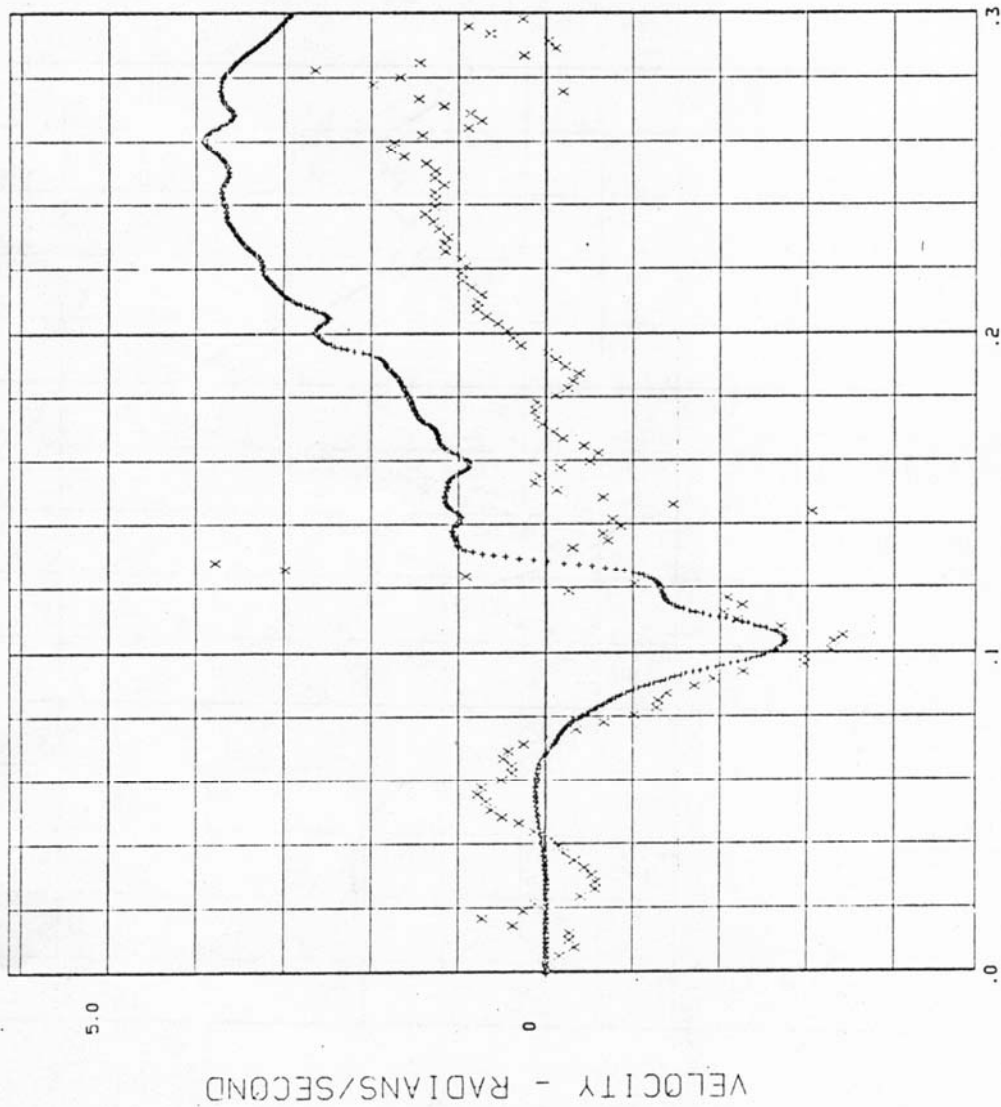
Fig. 9

Filtered (6)

3860.

.0940 129.9
(X) = RHA0XP

LX3579 H=00108
(+) = RHA0XS



20 JUN 80

TIME - SECONDS

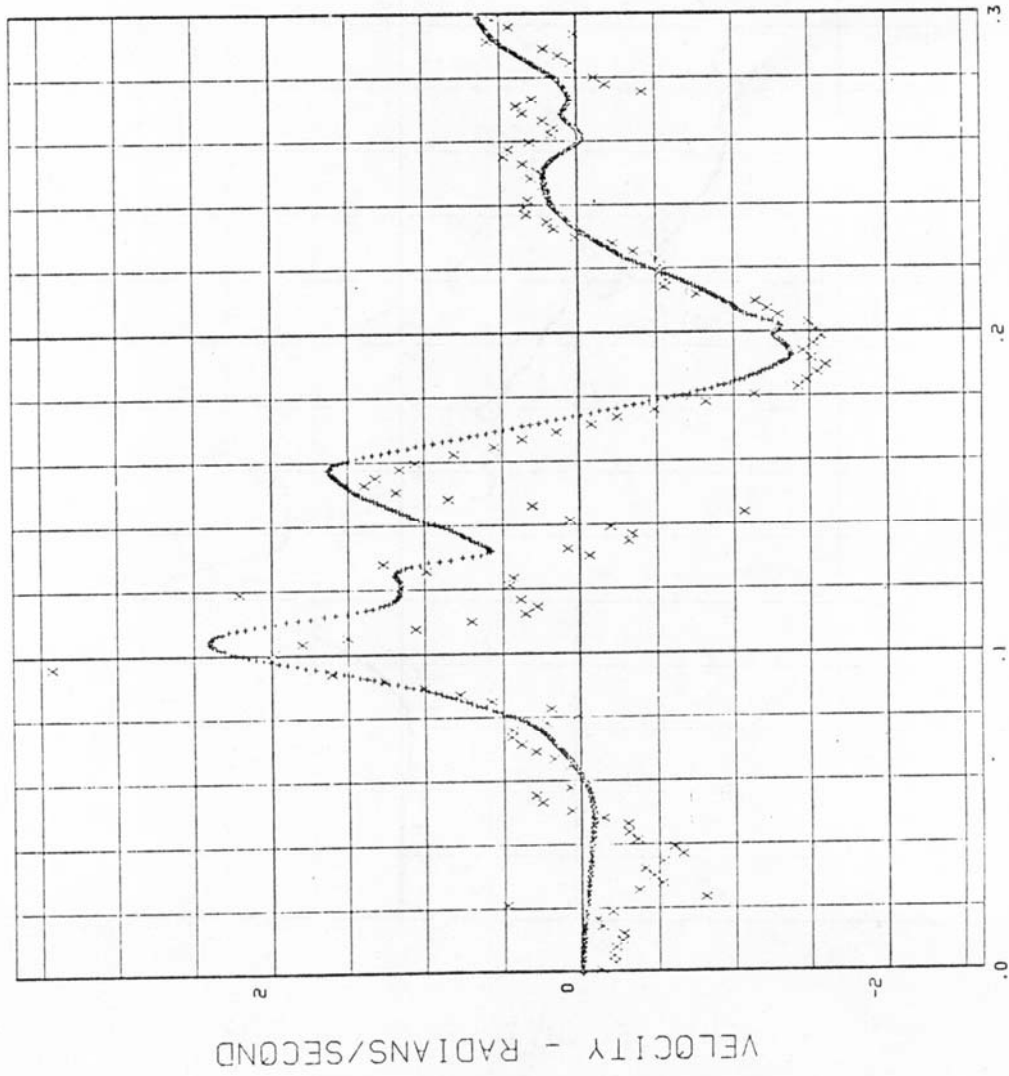
Fig. 10

Filtered (9)

3860.

.0940 129.9
(X) = RHCOXP

LX3579 H00108
(+) = RHCOXS



20 JUN 80

TIME - SECONDS

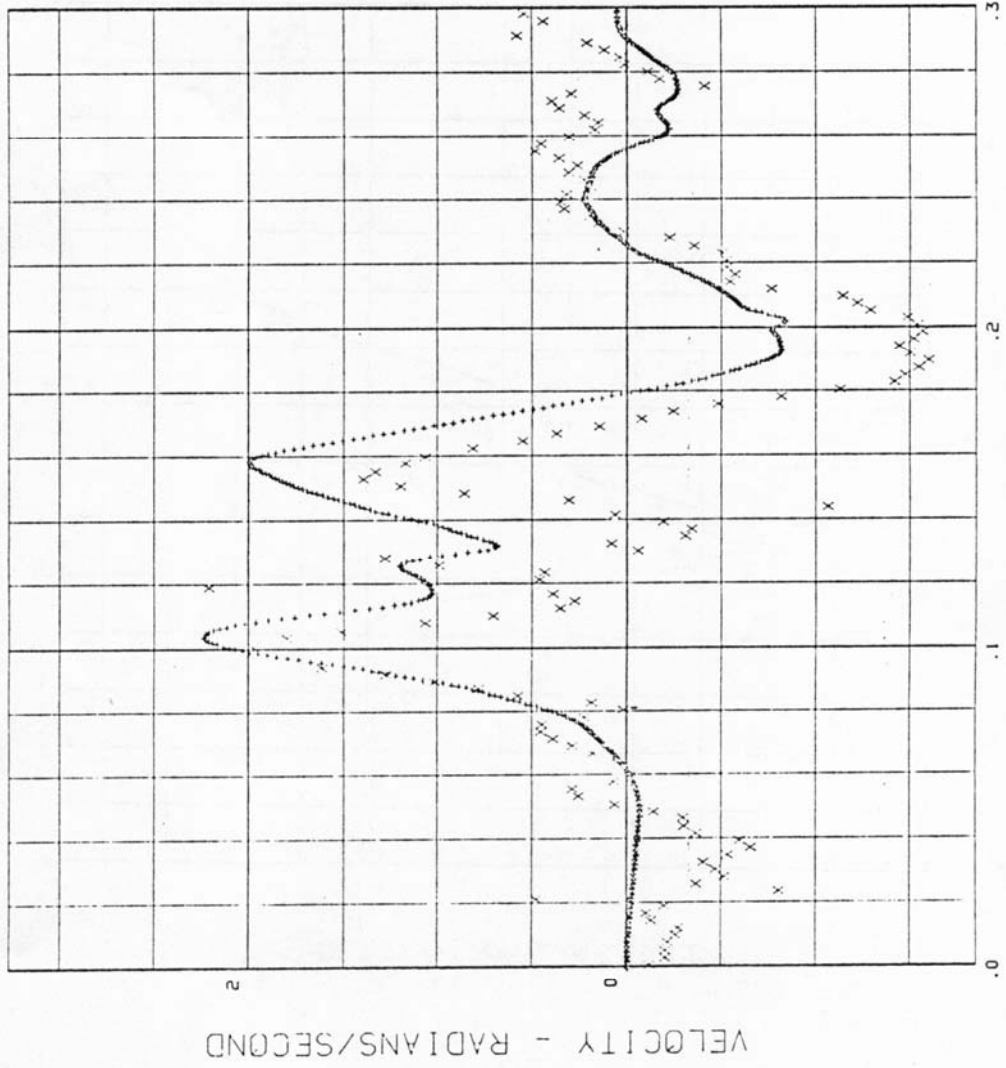
Fig. 11

Filtered (6)

3860.

.0940 129.9
(X) = RHC0XP

LX3579 H00108
(+) = RHC0XS



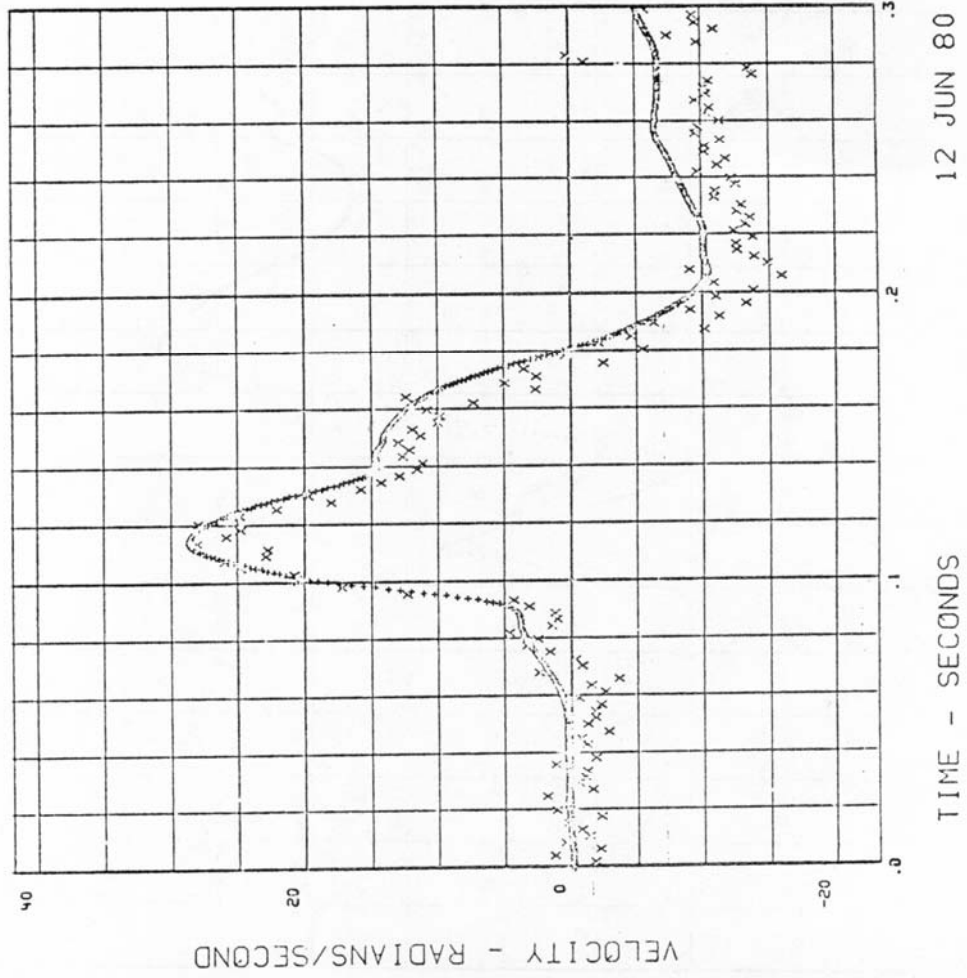
20 JUN 80

TIME - SECONDS

Fig. 12

unfiltered (9)

LX3584 H00108 .0923 138.9 4206.
[+] = RHBOXS [X] = RHBOXP

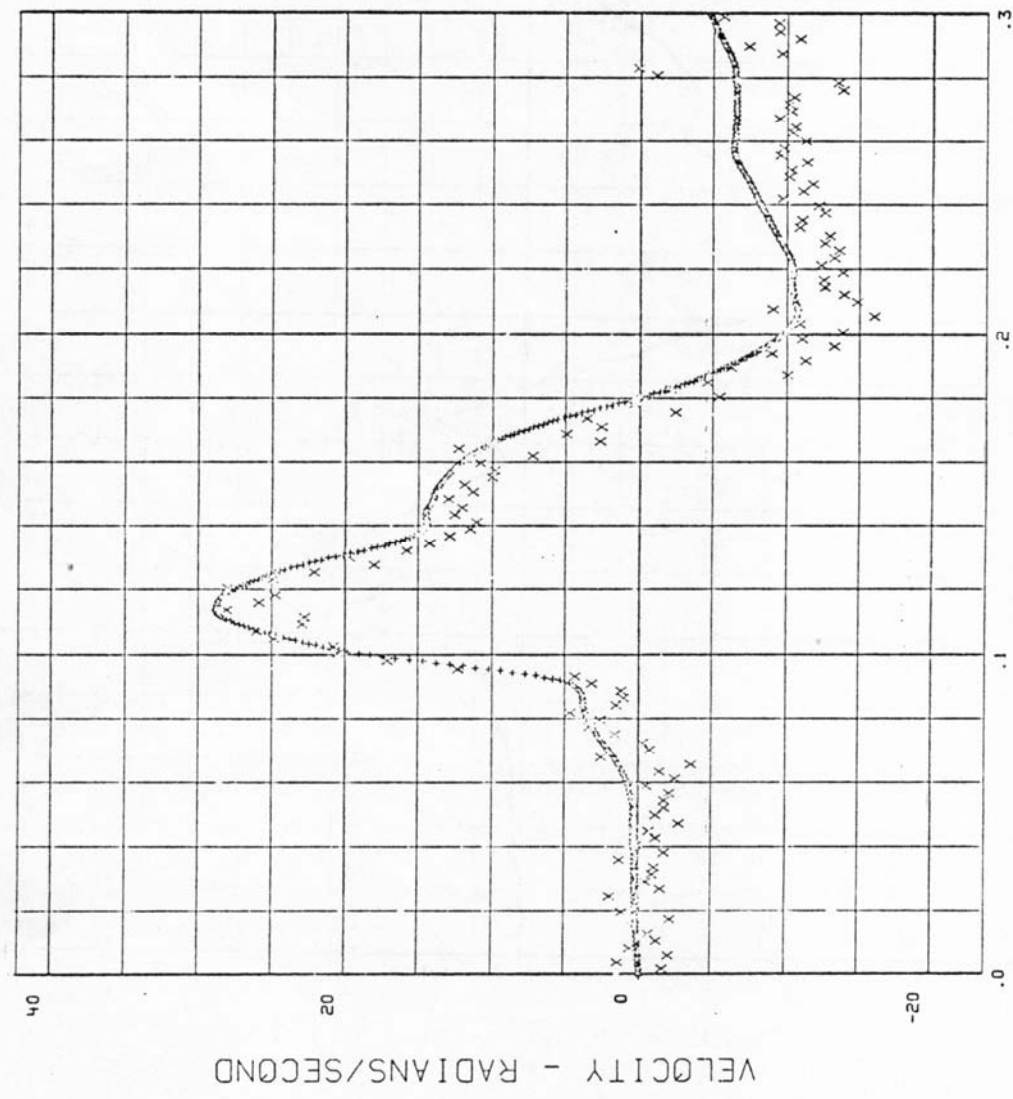


12 JUN 80

Fig. 13

unfiltered (6)

LX3584 H00108 .0923 138.9 4206.
(+) = RHBOXS (X) = RHBOXP



TIME - SECONDS 18 JUN 80

Fig. 14

Filtered (9)

4206.

138.9

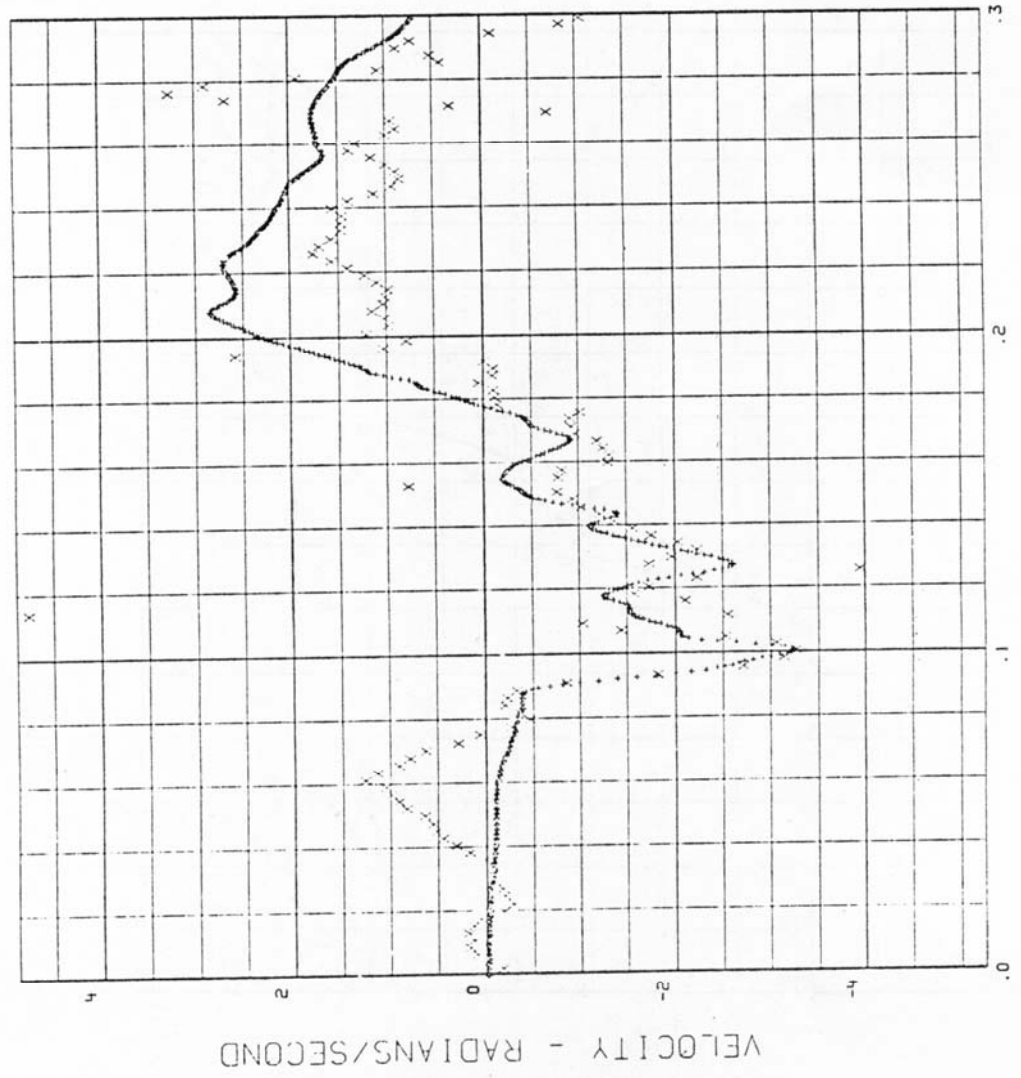
.0923

H00108

LX3584

(X) = RHACXP

(+) = RHACXS



20 JUN 80

TIME - SECONDS

Fig. 15

Filtered (6)

4206.

138.9

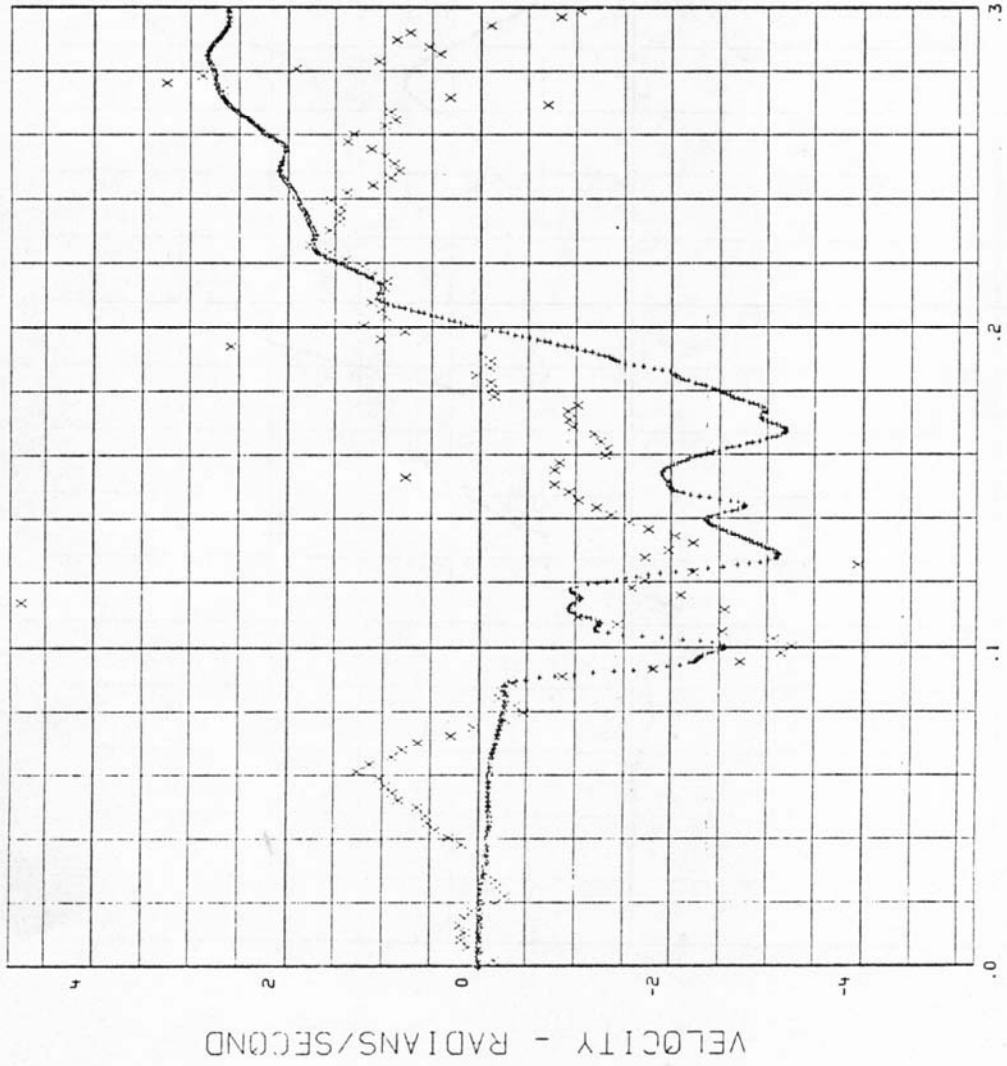
.0923

H00108

LX3584

(X) = RHA0XP

(+) = RHA0XS



20 JUN 80

TIME - SECONDS

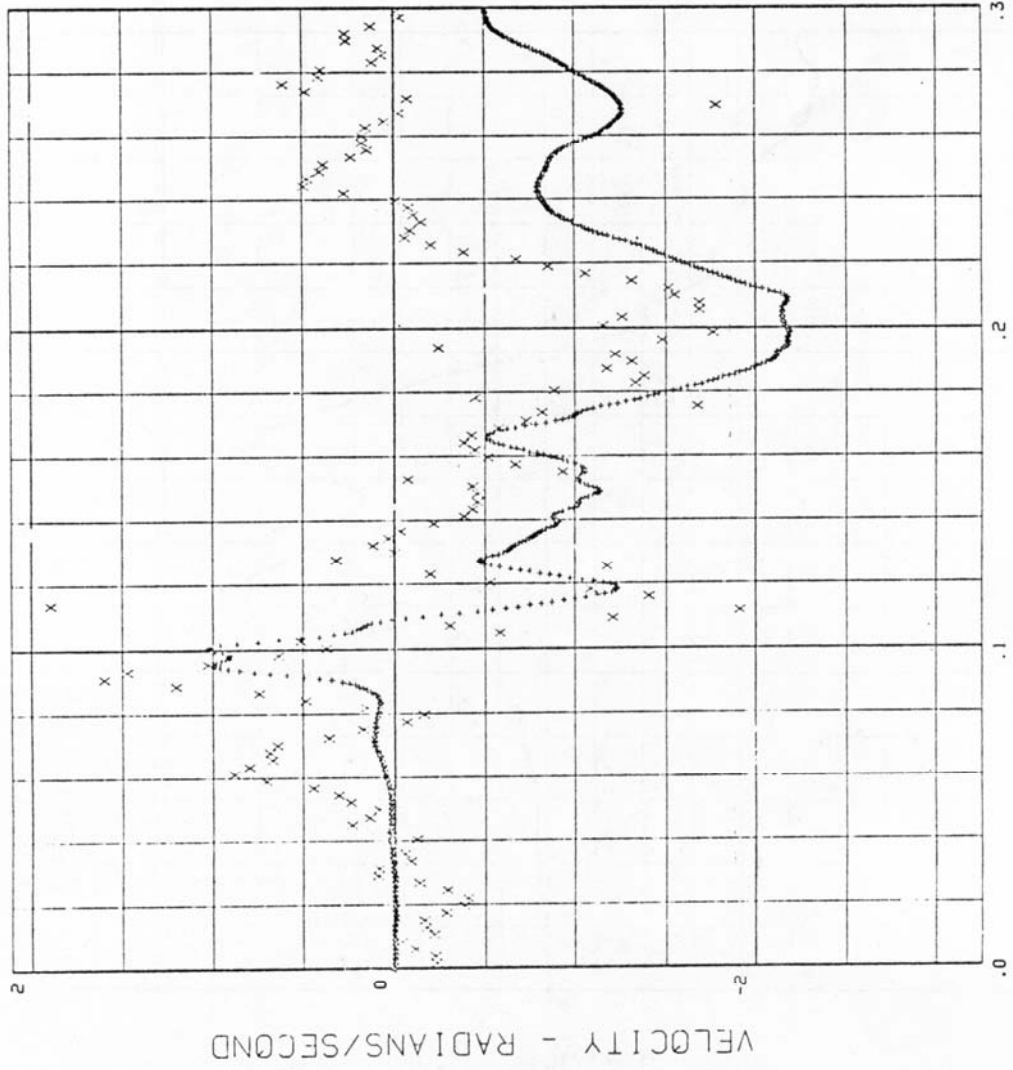
Fig. 16

Filtered (9)

4206.

.0923 (X) = RHCOXP

LX3584 H00108 (+) = RHCOXS

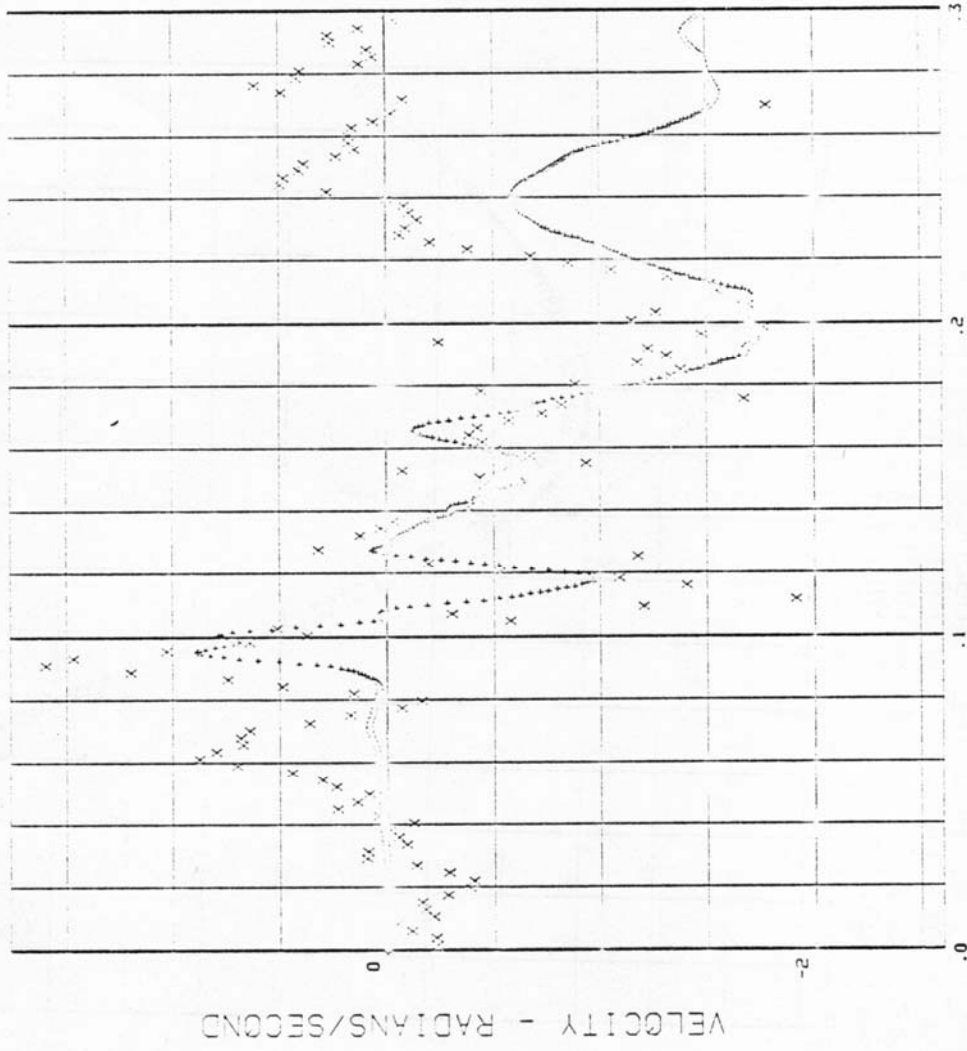


20 JUN 80

TIME - SECONDS

Fig. 17

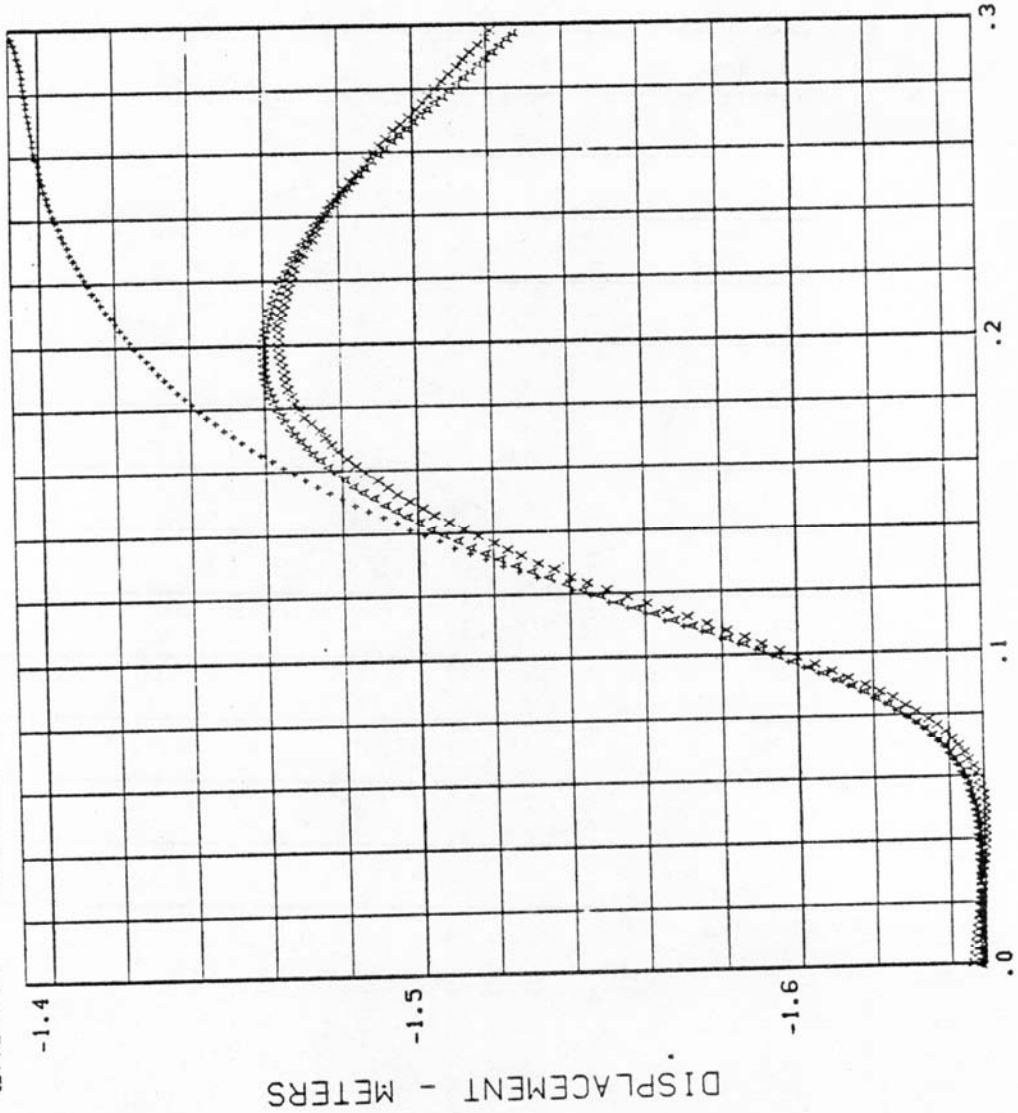
LX3584 H00108 .0923 138.9 4206.
(+) = RHCOXS (X) = RHCOXP



20 JUN 80

Fig. 18

RUN NO.	SYM. PLOTTED	SUBJECT	DELTA-T	ACC.	ONSET
LX3538	DAXS0A = (A)	H00108	.0020	71.1	1561.
LX3538	DAXS0P = (X)	H00108	.0022	71.1	1561.
LX3538	DAXS0S = (+)	H00108	.0020	71.1	1561.



TIME - SECONDS

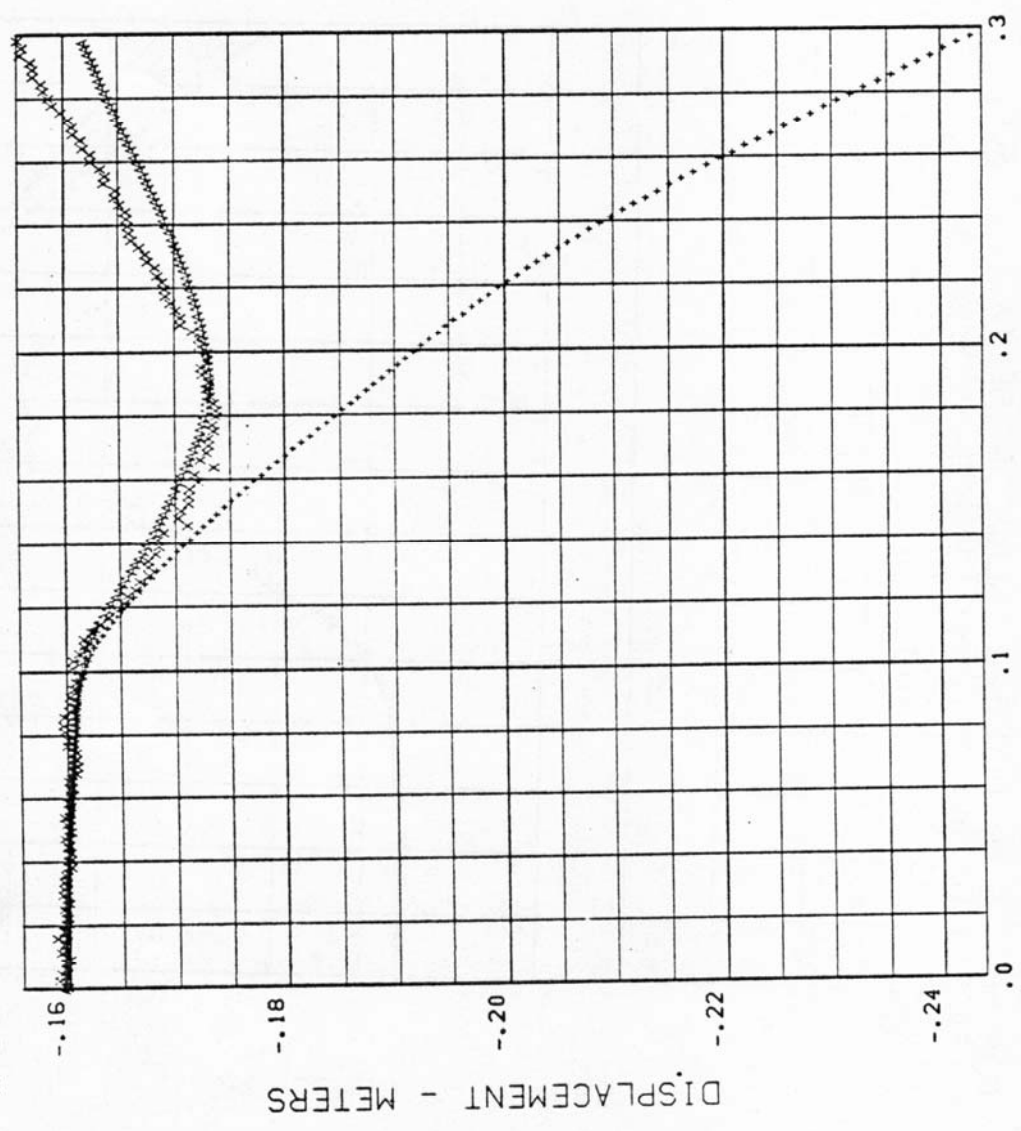
23 MAY 80

Fig. 19

```

RUN NO.      SYM. PLOTTED  SUBJECT  DELTA-T  ACC.  ONSET
LX3538      DAYS0A = (A)  H00108  .0020    71.1  1561.
LX3538      DAYS0P = (X)  H00108  .0022    71.1  1561.
LX3538      DAYS0S = (+)  H00108  .0020    71.1  1561.

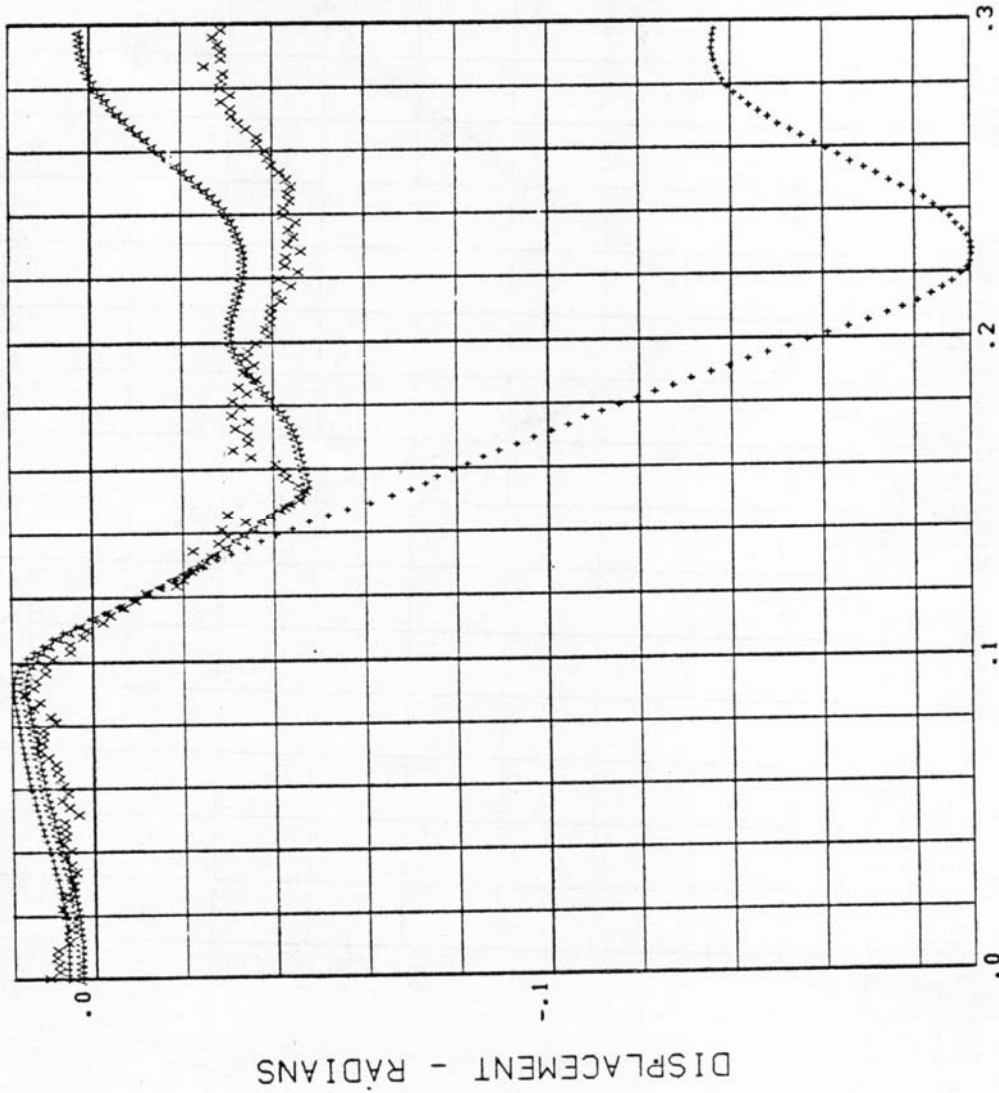
```



23 MAY 80

Fig. 20

RUN NO. SYM. PLOTTED SUBJECT DELTA-T ACC. ONSET
 LX3538 PHA0XA = (A) H00108 .0020 71.1 1561.
 LX3538 PHA0XP = (X) H00108 .0022 71.1 1561.
 LX3538 PHA0XS = (+) H00108 .0020 71.1 1561.

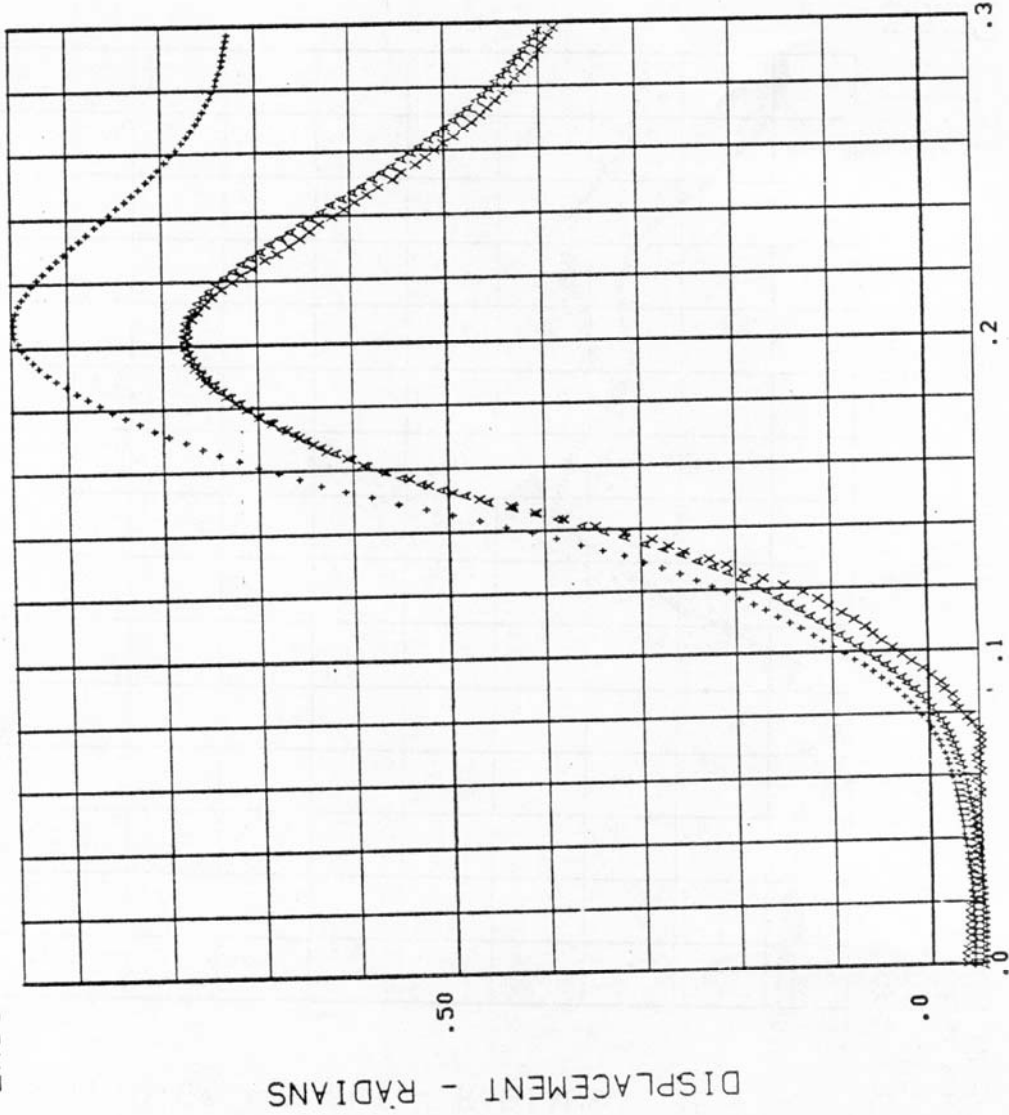


TIME - SECONDS

23 MAY 80

Fig. 22

RUN NO.	SYM. PLOTTED	SUBJECT	DELTA-T	ACC.	ONSET
LX3538	PHB02A = (A)	H00108	.0020	71.1	1561.
LX3538	PHB02P = (X)	H00108	.0022	71.1	1561.
LX3538	PHB02S = (+)	H00108	.0020	71.1	1561.

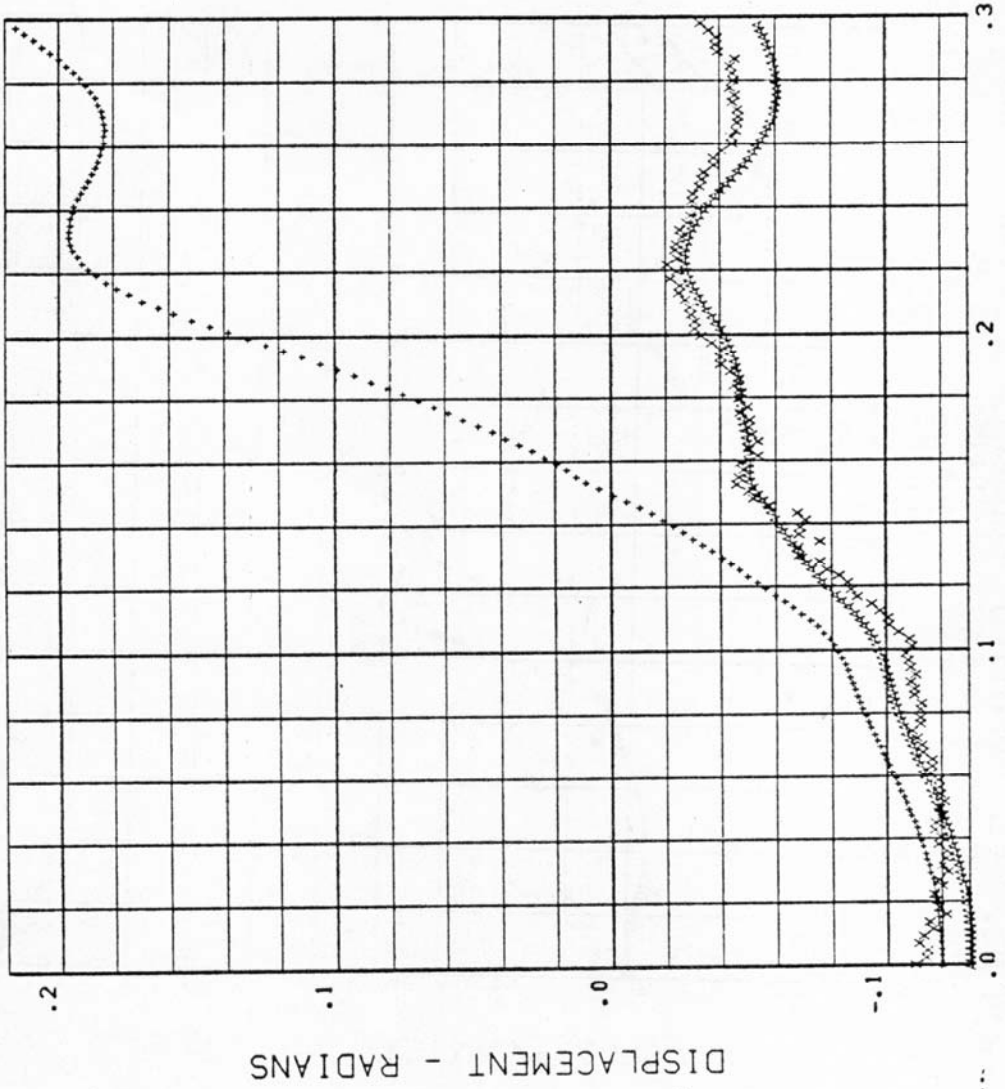


TIME - SECONDS

23 MAY 80

Fig.23

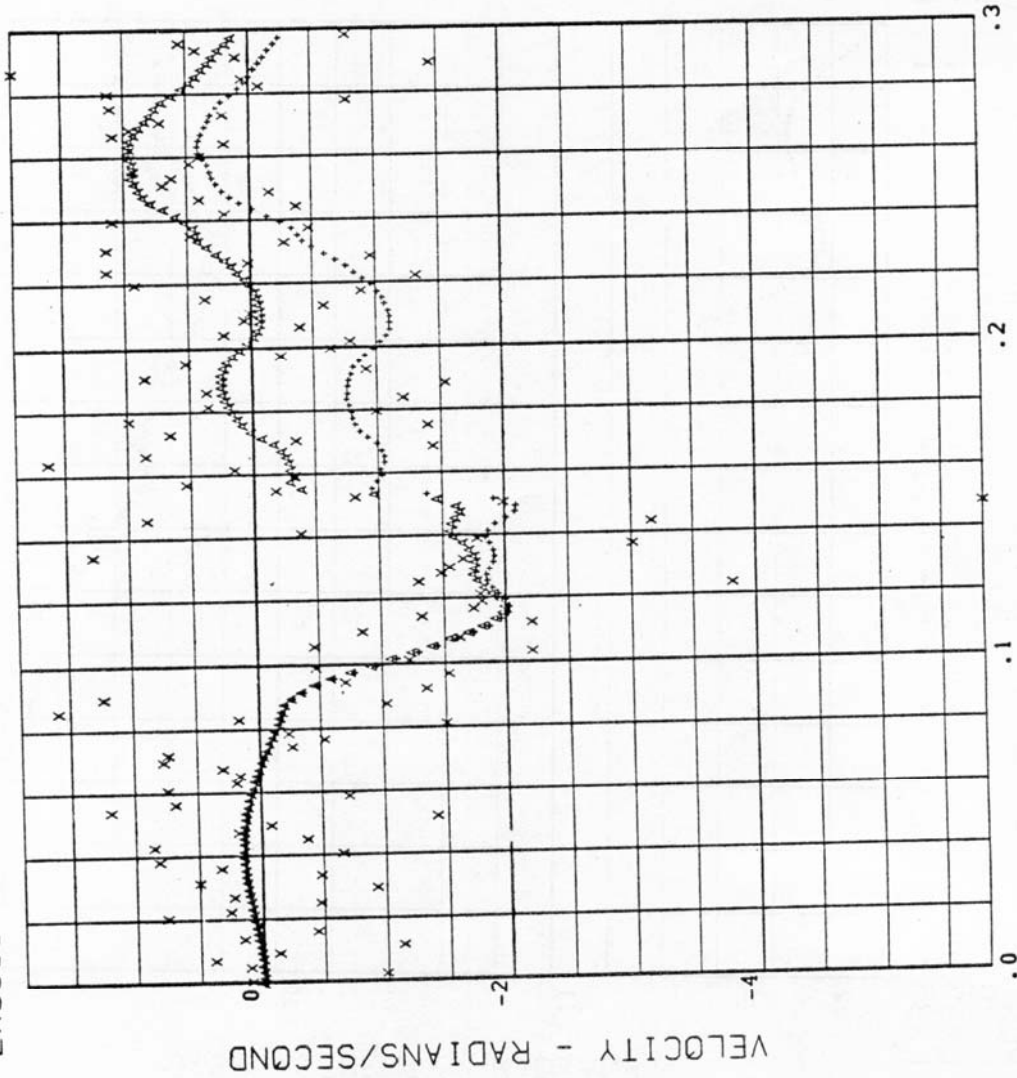
RUN NO.	SYM. PLOTTED	SUBJECT	DELTA-T	ACC.	ONSET
LX3538	PHC03A = (A)	H00108	.0020	71.1	1561.
LX3538	PHC03P = (X)	H00108	.0022	71.1	1561.
LX3538	PHC03S = (+)	H00108	.0020	71.1	1561.



TIME - SECONDS 23 MAY 80

Fig. 24

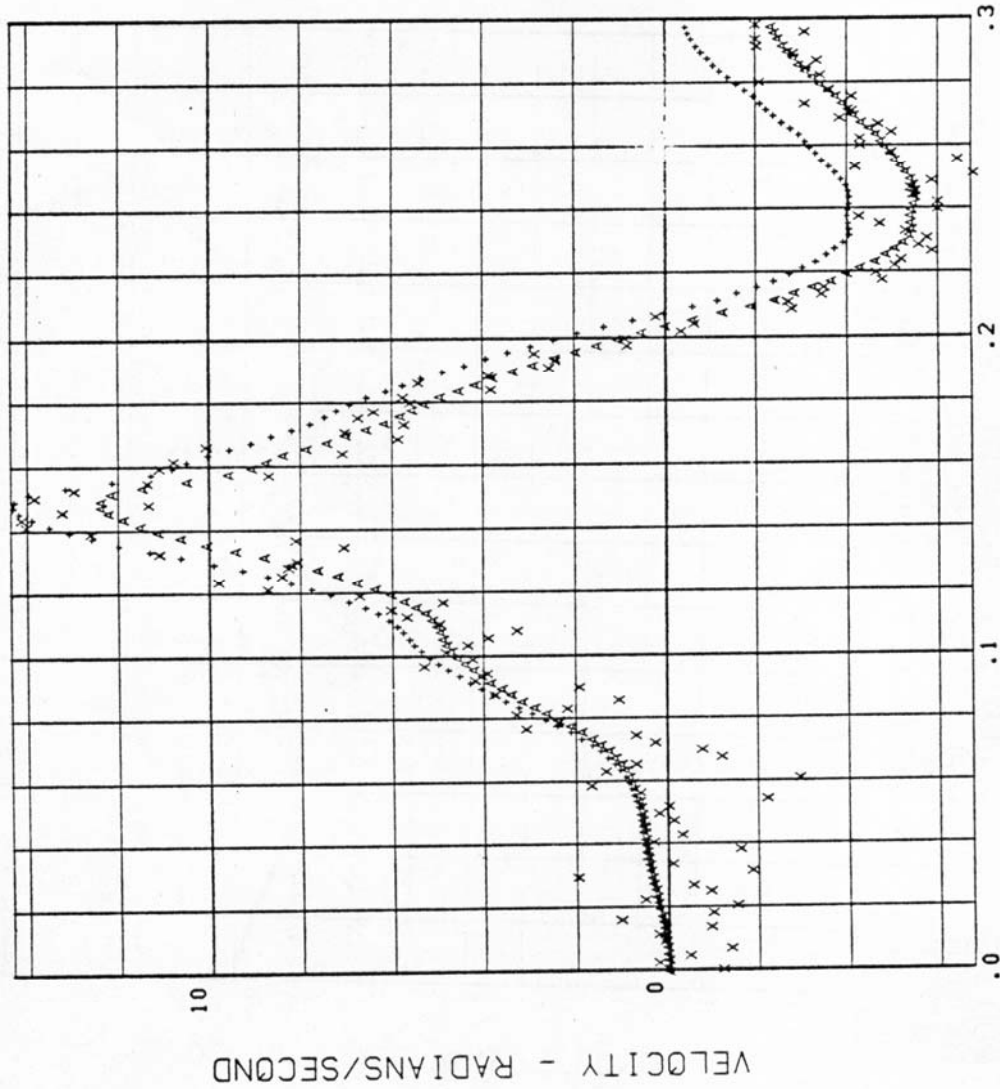
RUN NO.	SYM. PLOTTED	SUBJECT	DELTA-T	ACC.	ONSET
LX3538	RHA0XA = (A)	H00108	.0020	71.1	1561.
LX3538	RHA0XP = (X)	H00108	.0022	71.1	1561.
LX3538	RHA0XS = (+)	H00108	.0020	71.1	1561.



TIME - SECONDS 23 MAY 80

Fig. 25

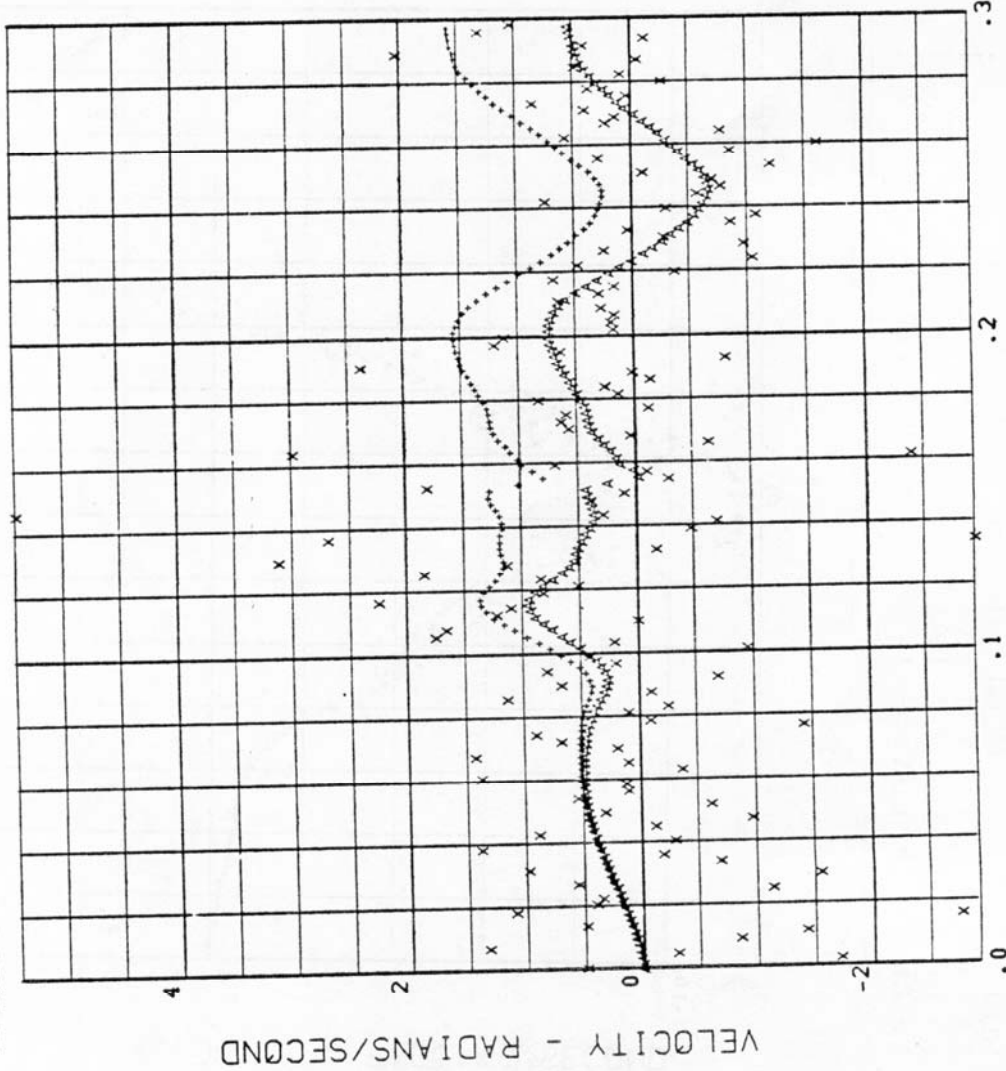
RUN NO. SYM. PLOTTED SUBJECT DELTA-T ACC. ONSET
 LX3538 RHBOXA = (A) H00108 :0020 71.1 1561.
 LX3538 RHBOXP = (X) H00108 :0022 71.1 1561.
 LX3538 RHBOXS = (+) H00108 :0020 71.1 1561.



TIME - SECONDS 23 MAY 80

Fig. 26

RUN NO. SYM. PLOTTED SUBJECT DELTA-T ACC. ONSET
 LX3538 RHC0XA = (A) H00108 : 0020 71:1 1561:
 LX3538 RHC0XP = (X) H00108 : 0022 71:1 1561:
 LX3538 RHC0XS = (+) H00108 : 0020 71:1 1561:



TIME - SECONDS 23 MAY 80

Fig. 27